Photonic band-gap crystals

J. Phys.: Condens. Matter 5 (1993) 2443–2460. Printed in the UK

REVIEW ARTICLE

Photonic band-gap crystals

E Yablonovitch

Department of Electrical Engineering, University of California at Los Angeles, Los Angeles, CA 90024-1594, USA

Received 11 January 1993

Abstract. The analogy between electromagnetic wave propagation in multidimensionally periodic structures and electron wave propagation in real crystals has proven to be a very fruitful one. Initial efforts were motivated by the prospect of a photonic band gap, a frequency band in three-dimensional dielectric structures in which electromagnetic waves are forbidden, irrespective of propagation direction in space. Today many new ideas and applications are being persued in two and three dimensions, and in metallic, dielectric and acoustic structures, etc.

In this paper, we review the early motivations for this work, which were derived from the need for a photonic band gap in quantum optics. This led to a series of experimental and theoretical searches for the elusive photonic band-gap structures, those three-dimensionally periodic dielectric structures which are to photon waves what semiconductor crystals are to electron waves. Then we describe how the photonic semiconductor can be 'doped', producing tiny electromagnetic cavities. Finally, we will summarize some of the anticipated implications of photonic band structure for quantum electronics and the prospects for the creation of photonic crystals in the optical domain.

1. Introduction

In this review we will pursue the rather appealing analogy [1,2] between the behaviour of electromagnetic waves in artificial three-dimensionally periodic, dielectric structures and the rather more familiar behaviour of electron waves in natural crystals.

These artificial two- and three-dimensionally periodic structures we will call 'photonic crystals'. The familiar nomenclature of real crystals will be carried over to the electromagnetic case. This means that the concepts of reciprocal space, Brillouin zones, dispersion relations, Bloch wavefunctions, Van Hove singularities, etc., must now be applied to photon waves. It makes sense then to speak of photonic band structure and of a photonic reciprocal space, which has a Brillouin zone approximately 1000 times smaller than the Brillouin zone of the electrons. Owing to the periodicity, photons can develop an effective mass, but this is in no way unusual, since it occurs even in one-dimensionally periodic, optically layered, structures. We will frequently leap back and forth between the conventional meaning of a familiar concept like 'conduction band' and its new meaning in the context of photonic band structure.

Under favourable circumstances, a 'photonic band gap' can open up, a frequency band in which electromagnetic waves are forbidden, irrespective of propagation direction in space. Inside a photonic band gap, optical modes, spontaneous emission and zero-point fluctuations are all absent. Because of its promised ability to control spontaneous emission of light in quantum optics, the pursuit of a photonic band gap has been a major motivation for studying photonic band structure.

0953-8984/93/162443+18$07.50

2. Motivation

Spontaneous emission of light is a major natural phenomenon which is of great practical and commercial importance. For example, in semiconductor lasers, spontaneous emission is the major sink for threshold current, which must be surmounted in order to initiate lasing. In heterojunction bipolar transistors (HBTs), which are non-optical devices, spontaneous emission nevertheless rears its head. In some regions of the transistor current–voltage characteristic, spontaneous optical recombination of electrons and holes determines the HBT current gain. In solar cells, surprisingly, spontaneous emission fundamentally determines the maximum available output voltage. We will also see that spontaneous emission determines the degree of photon-number-state squeezing, an important new phenomenon [3] in the quantum optics of semiconductor lasers. Thus the ability to control spontaneous emission of light is expected to have a major impact on technology.

The easiest way to understand the effect of a photonic band gap on spontaneous emission is to take note of Fermi's golden rule. The downward transition rate w between the filled and empty atomic levels is given by

$$w = (2\pi/\hbar)|V|^2\rho(E) \tag{1}$$

where $|V|$ is sometimes called the zero-point Rabi matrix element and $\rho(E)$ is the density of the final states per unit energy. In spontaneous emission, the density of final states is the density of optical modes available to the photon. If there are no optical modes available, there will be no spontaneous emission.

Before the 1980s, spontaneous emission was often regarded as a natural and inescapable phenomenon, one over which no control was possible. In spectroscopy it gave rise to the term 'natural linewidth'. However, in 1946, an overlooked note by Purcell [4] on nuclear spin levels had already indicated that spontaneous emission could be controlled. In the early 1970s, interest in this phenomenon was reawakened by the surface-adsorbed dye molecule fluorescence studies [5] of Drexhage. Indeed, during the mid-1970s, Bykov proposed [6] that one-dimensional periodicity inside a coaxial line could influence spontaneous emission. The modern era of inhibited spontaneous emission dates from the Rydberg atom experiments of Kleppner. A pair of metal plates acts as a waveguide, with a cut-off frequency for one of the two polarizations, as shown in figure 1. Rydberg atoms are atoms in very-high-lying principal-quantum-number states, which can spontaneous emit in the microwave region of wavelengths. Kleppner *et al* [7] showed that Rydberg atoms in a metallic waveguide could be prevented from undergoing spontaneous decay. There were no modes available below the waveguide cut-off.

There is a problem with metallic waveguides, however. They do not scale well into optical frequencies. At high frequencies, metals become more and more lossy. These dissipative losses allow for virtual modes, even at frequencies that would normally be forbidden. Therefore, it makes sense to consider structures made of positive-dielectric-constant materials such as glasses and insulators, rather than metals. These can have very low dissipation, even all the way up to optical frequencies. This is ultimately exemplified by optical fibres, which allow light propagation over many kilometres with negligible losses. Such positive-dielectric-constant materials can have an almost purely real dielectric response with low resistive losses. If arrayed into a three-dimensionally periodic dielectric structure, a photonic band gap should be possible, employing a purely real, reactive, dielectric response.

The benefits of such a photonic band gap for direct-gap semiconductors are illustrated in figure 2. On the right-hand side is a plot of the photon dispersion (frequency versus

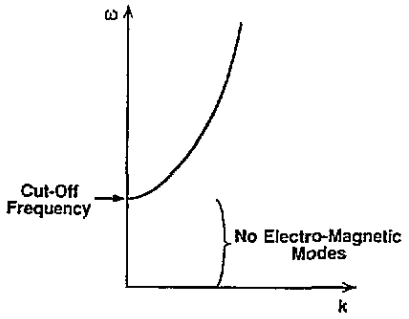

Figure 1. Electromagnetic wave dispersion between a pair of metal plates. The waveguide dispersion has a cut-off frequency below which there are no electromagnetic modes, and there is no spontaneous emission allowed.

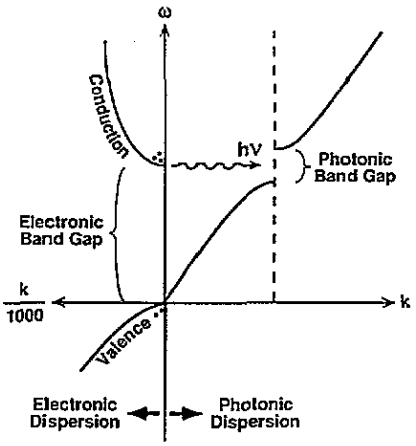

Figure 2. On the right is the electromagnetic dispersion, with a forbidden gap at the wavevector of the periodicity. On the left is the electron wave dispersion typical of a direct-gap semiconductor, the dots representing electrons and holes. Since the photonic band gap straddles the electronic band edge, electron–hole recombination into photons is inhibited. The photons have no place to go.

wavevector). On the left-hand side, sharing the same frequency axis, is a plot of the electron dispersion, showing conduction and valence bands appropriate to a direct-gap semiconductor. Since atomic spacings are 1000 times shorter than optical wavelengths, the electron wavevector must be divided by 1000 in order to fit on the same graph with the photon wavevectors. The dots in the conduction and valence bands are meant to represent electrons and holes respectively. If an electron were to recombine with a hole, they would produce a photon at the electronic band-edge energy. As illustrated in figure 2, if a photonic band gap straddles the electronic band edge, then the photon produced by electron–hole recombination would have no place to go. The spontaneous radiative recombination of electrons and holes would be inhibited. As can be imagined, this has far-reaching implications for semiconductor photonic devices.

One of the most important applications of inhibited spontaneous emission is likely to be the enhancement of photon-number-state squeezing, which has been playing an increasing role in quantum optics lately. The form of squeezing introduced by Yamamoto [3] is particularly appealing, in that the active element producing the squeezing effect is none other than the common resistor. When an electrical current flows, it generally carries the noise associated with the graininess of the electron charge, called shot noise. The corresponding mean-square current fluctuations are

$$\langle(\Delta i)^2\rangle = 2ei\Delta f \tag{2}$$

where i is the average current flow, e is the electronic charge and Δf is the noise bandwidth. While equation (2) applies to many types of random physical processes, it is far from universal. Equation (2) requires that the passage of electrons in the current flow be a random Poisson process. As early as 1954, Van der Ziel [8], in an authoritative book called *Noise*, pointed out that good-quality metal film resistors, when carrying a current, generally exhibit much less noise than that given by equation (2). Apparently, the flow of electrons in

the Fermi sea of a metallic resistor represents a highly correlated process. Far from being a random process, the electrons apparently sense one another, producing shot noise far below that in equation (2) (so low as to be difficult to measure and to distinguish from thermal or Johnson noise). Sub-Poisson shot noise has the following meaning: Suppose the average flow consists of 10 electrons per nanosecond. Under random flow, the count in successive nanoseconds could sometimes vary from about 8 to 12 electrons. With good-quality metal film resistors, the electron count would be 10 for each and every nanosecond.

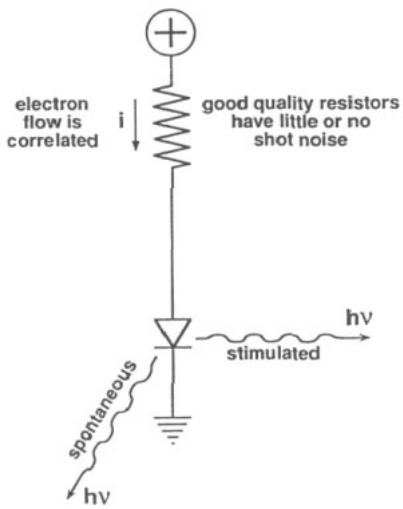

Figure 3. A high-quantum-efficiency laser diode converts the correlated flow of electrons from a low-shot-noise resistor into photon-number-state squeezed light. Random spontaneous emission outside the desired cavity mode limits the attainable noise reduction.

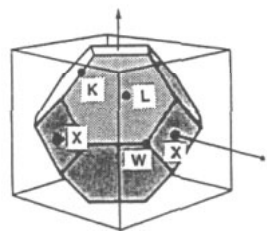

Figure 4. The face-centred cubic Brillouin zone in reciprocal space.

Yamamoto put this property to good use by driving a high-quantum-efficiency laser diode with such a resistor as shown in figure 3. Suppose the laser diode quantum efficiency into the cavity mode were 100%. Then for each electron passing through the resistor there would be one photon emitted into the laser cavity mode. A correlated stream of photons is produced whose statistical properties are unprecedented since Einstein's interpretation of the photoelectric effect. If the photons are used for optical communication, then a receiver would detect exactly 10 photoelectrons each nanosecond. If 11 photons were detected, it would be no mere random fluctuation, but would represent an intentional signal. Thus information in an optical communications signal could be encoded at the level of individual photons. The name photon-number-state squeezing is associated with the fixed photon number per unit time interval. Expressed differently, the bit error rate in optical communication can be diminished by squeezing.

There is a limitation to the squeezing, however. The quantum efficiency into the lasing mode is not 100%. The 4π steradians outside the cavity mode can capture a significant amount of random spontaneous emission. If unwanted electromagnetic modes captured 50% of the excitation, then the maximum noise reduction in squeezing would be only 3 dB. Therefore, it is necessary to minimize the spontaneous recombination of electrons and holes into modes other than the lasing mode. If such random spontaneous events were reduced

to 1%, allowing 99% quantum efficiency into the lasing mode, the corresponding noise reduction would be 20 dB, well worth fighting for. Thus we see that control of spontaneous emission is essential for deriving the full benefit from photon-number-state squeezing.

We have motivated the study of photonic band structure for its applications in quantum optics and optical communications. Positive dielectric constants and fully three-dimensional forbidden gaps were emphasized. It is now clear that the generality of artificial, multidimensional, band-structure concepts allows for other types of waves, other materials and various lower-dimensional geometries, limited only by imagination and need.

3. Search for the photonic band gap

Having decided to create a photonic band gap in three dimensions, we need to settle on a particular three-dimensionally periodic geometry. For electrons, the three-dimensional crystal structures come from nature. Several hundred years of mineralogy and crystallography have classified the naturally occurring three-dimensionally periodic lattices. For photonic band gaps, however, we must create an artificial structure using our imagination.

The face centred cubic (FCC) lattice appears to be favoured for photonic band gaps, and was suggested independently by Yablonovitch [1] and John [2] in their initial proposals. Let us consider the FCC Brillouin zone (BZ) as illustrated in figure 4. Various special points on the surface of the BZ are marked. Closest to the centre is the L point, oriented towards the body diagonal of the cube. Farthest away is the W point, a vertex where four plane waves are degenerate (which will cause problems later on). In the cubic directions are the familiar X points.

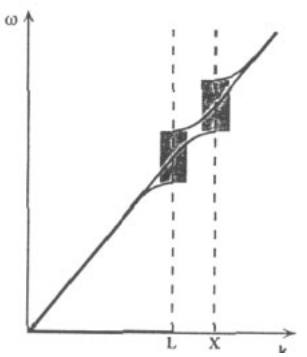

Figure 5. The forbidden gap (shaded) at the L point is centred at a frequency ~ 14% lower than the X point forbidden gap. Therefore, it is difficult to create a forbidden frequency band overlapping all points along the surface of the Brillouin zone.

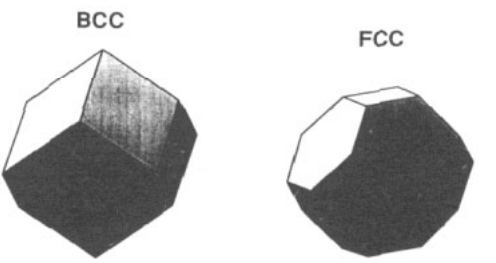

Figure 6. Two common Brillouin zones for body-centred and face-centred cubic. The FCC case deviates least from a sphere, favouring a common overlapping band in all directions of space.

Consider a plane wave in the X direction. It will sense the periodicity in the cubic direction, forming a standing wave, and opening up a forbidden gap as indicated by the shading in figure 5. Suppose, on the other hand, that the plane wave is going in the L direction. It will sense the periodicity along the cubic body diagonal, and a gap will form in that direction as well. But the wavevector to the L point is about 14% smaller than the

wavevector to the X point. Therefore, the gap at L is likely to be centred at a 14% smaller frequency than the gap at X. If the two gaps are not wide enough, they are unlikely to overlap in frequency. In figure 5 as shown, the two gaps barely overlap. This is the main problem in achieving a photonic band gap. It is difficult to ensure that a common frequency overlap is assured for all possible directions in reciprocal space.

The lesson from figure 5 is that the Brillouin zone should most closely resemble a sphere in order to increase the likelihood of a common frequency overlap in all directions of space. Therefore, let us look at the two common Brillouin zones in figure 6, the FCC BZ and the body-centred cubic (BCC) BZ. The BCC BZ has 'pointed' vertices, which make it difficult to achieve a common frequency overlap in all directions. Likewise, most other common BZs deviate even farther from a spherical shape. Among all the common BZs the FCC has the least percentage deviation from a sphere. Therefore up until now most photonic band gaps in three dimensions have been based on the FCC lattice. (There has been a report recently of a photonic band gap in a simple cubic geometry [9]).

The photonic band gap is different from the idea of a one-dimensional stop band as understood in electrical engineering. Rather, the photonic band gap should be regarded as a stop band with a common frequency overlap in all 4π steradians of space. The earliest antecedent to photonic band structure, dating back to 1914 [10] and Sir Lawrence Bragg, is the 'dynamical theory of x-ray diffraction'. Nature gives us face-centred cubic crystals and x-rays are *bona fide* electromagnetic waves. As early as 1914, narrow stop bands were known to open up. Therefore, what was missing?

The refractive-index contrast for x-rays is tiny, generally less than one part in 10^4. The forbidden x-ray stop bands form extremely narrow rings on the facets of the BZ. As the index contrast is increased, the narrow forbidden rings open up, eventually covering an entire facet of a BZ and ultimately covering all directions in reciprocal space. We will see that this requires an index contrast $\gtrsim 2:1$. The high index contrast is the main new feature of photonic band structure beyond dynamical x-ray diffraction. In addition, we will see that electromagnetic wave polarization, which is frequently overlooked for x-rays, will play a major role in photonic band structure.

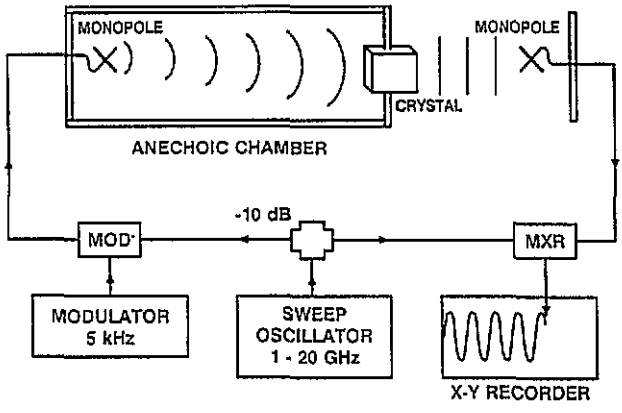

Figure 7. A homodyne detection system for measuring phase and amplitude in transmission through the photonic crystal under test. A sweep oscillator feeds a 10 dB splitter. Part of the signal is modulated (MOD) and then propagated as a plane wave through the test crystal. The other part of the signal is used as local oscillator for the mixer (MXR) to measure the amplitude change and phase shift in the crystal. Between the mixer and the X–Y recorder is a lock-in amplifier (not shown).

In approaching this subject, we adopted an empirical viewpoint. We decided to make photonic crystals on the scale of microwaves, and then we tested them using sophisticated coherent microwave instruments. The test set-up, shown in figure 7, is what we would call in optics a Mach–Zender interferometer. It is capable of measuring phase and amplitude in

transmission through the microwave-scale photonic crystal. In principle, one can determine the frequency versus wavevector dispersion relations from such coherent measurements. Later on we used a powerful commercial instrument for this purpose, the HP 8510 Network Analyser. The philosophy of the experiments was to measure the forbidden gap in all possible internal directions in reciprocal space. Accordingly, the photonic crystal was rotated and the transmission measurements repeated. Owing to wavevector matching along the surface of the photonic crystal, some internal angles could not be accessed. To overcome this, large microwave prisms, made out of poly(methy methacrylate), were placed on either side of the test crystal in figure 7.

Early on the question arose, of what material the photonic crystal should be made? The larger the refractive-index contrast, the easier it would be to find a photonic band gap. In optics, however, the largest practical index contrast is that of the common semiconductors, Si and GaAs, with a refractive index $n = 3.6$. If that index was inadequate, then photonic crystals would probably never fulfill the goal of being useful in optics. Therefore, we decided to restrict the microwave refractive index to 3.6, and the microwave dielectric constant to $n^2 = 12$. A commercial microwave material, Emerson & Cumming Stycast 12, was particularly suited to the task since it was machinable with carbide tool bits. Any photonic band structure that was found in this material could simply be scaled down in size and would have the identical dispersion relations at optical frequencies and optical wavelengths.

With regard to the geometry of the photonic crystal, there are a universe of possibilities. So far, the only restriction we have made is towards face-centred cubic lattices. It turns out that a crystal, with an FCC BZ in reciprocal space, as shown in figure 4, is composed of FCC Wigner–Seitz (WS) unit cells in real space as shown in figure 8. The problem of creating an arbitrary FCC dielectric structure reduces to the problem of filling the FCC WS real-space unit cell with an arbitrary spatial distribution of dielectric material. Real space is then filled by repeated translation and close packing of the WS unit cells. The decision before us, is what to put inside the FCC Wigner-Seitz cells? There are an infinite number of possible FCC lattices, since anything can be put inside the fundamental repeating unit. In x-ray language, we have to find a 'form factor' for the WS unit cell that would produce a crystal with a photonic band gap.

This question provoked strenuous difficulties and false starts over a period of several years before finally being solved. In the first years of this research, we were unaware of how difficult the search for a photonic band gap would be. A number of FCC crystal structures were proposed, each representing a different choice for filling the rhombic dodecahedron FCC WS cells in real space. For example, the very first suggestion [1] was to make a three-dimensional 'checker-board' as in figure 9, in which cubes were inscribed inside the FCC WS real-space cells in figure 8. Later on, the experiments [11] adopted spherical 'atoms' centred inside the FCC WS cell were composed of precision Al_2O_3 spheres, $n \sim 3.06$, each ~ 6 mm in diameter. This structure was tested at a number of filling ratios from close packing to very dilute. Nevertheless, it always failed to produce a photonic band gap!

Then we tested the inverse structure in which spherical voids were inscribed inside the FCC WS real-space cell. These could be easily fabricated by drilling hemispheres onto the opposite faces of a dielectric sheet with a spherical drill bit as shown in figure 10. When the sheets were stacked up so that the hemispheres faced one another, the result was an FCC array of spherical voids inside a dielectric block. These were also tested over a wide range of filling ratios by progressively increasing the diameter of the hemispheres. These also failed to produce a photonic band gap!

The typical failure mode is illustrated in figure 11. As expected the 'conduction band'

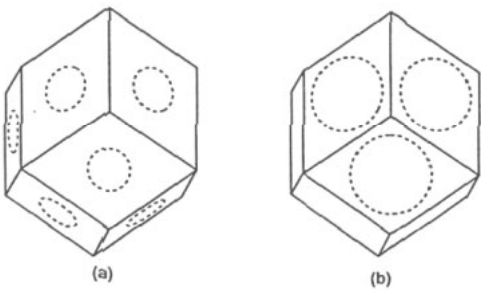

Figure 8. The Wigner–Seitz real-space unit cell of the FCC lattice is a rhombic dodecahedron. (*a*) Slightly oversized spherical voids are inscribed into the unit cell, breaking through the faces, as illustrated by broken circles. (*b*) The WS cell structure possessing a photonic band gap. Cylindrical holes are drilled through the top three facets of the rhombic dodecahedron and exit through the bottom three facets. The resulting atoms are roughly cylindrical, and have a preferred axis in the vertical direction.

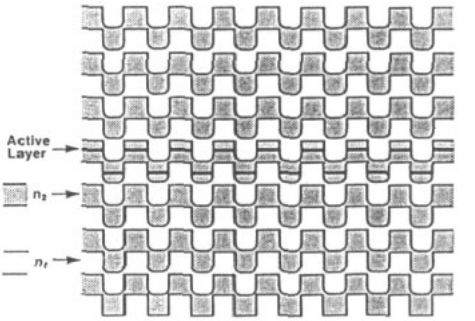

Figure 9. A face-centred cubic crystal in which the individual WS cells are inscribed with cubes stacked in a three-dimensional 'checker-board'.

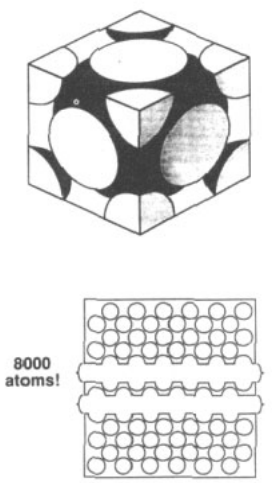

Figure 10. Construction of FCC crystals consisting of spherical voids. Hemispherical holes drilled on both faces of a dielectric sheet. When the sheets are stacked up, the hemispheres meet, producing an FCC crystal.

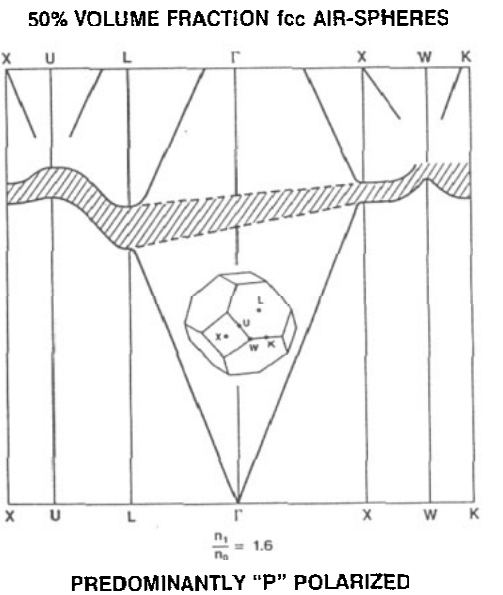

Figure 11. Typical semi-metallic band structure for a photonic crystal with no photonic band gap (50% volume fraction FCC 'air-atoms', predominantly p polarized, $n_1/n_0 = 1.6$). An overlap exists between the conduction band at L and the valence band at W.

at the L point falls at a low frequency, while the 'valence band' at the W point falls at a high frequency. The overlap of the bands at L and W results in a band structure that is best described as 'semi-metallic'.

The empirical search for a photonic band gap led nowhere until we tested a spherical void structure with oversized voids breaking through the walls of the WS unit cell as shown in figure 8(*a*). For the first time, the measurements seemed to indicate a photonic band gap and we published [11] the band structure shown in figure 12. There appeared to be a narrow gap, centred at 15 GHz, and forbidden for both possible polarizations. Unbeknown to us, however, figure 12 harboured a serious error. Instead of a gap at the W point, the conduction and valence bands crossed at that point, allowing the bands to touch. This produced a pseudo-gap with zero density of states but *no* frequency width. The error arose due to the limited size of the crystal. The construction of crystals with $\sim 10^4$ atoms required tens of thousands of holes to be drilled. Such a three-dimensional crystal was still only 12 cubic units wide, limiting the wavevector resolution, and restricting the dynamic range in transmission. Under these conditions, it was experimentally difficult to notice a conduction–valence band degeneracy that occurred at an isolated point in k-space, such as the W point.

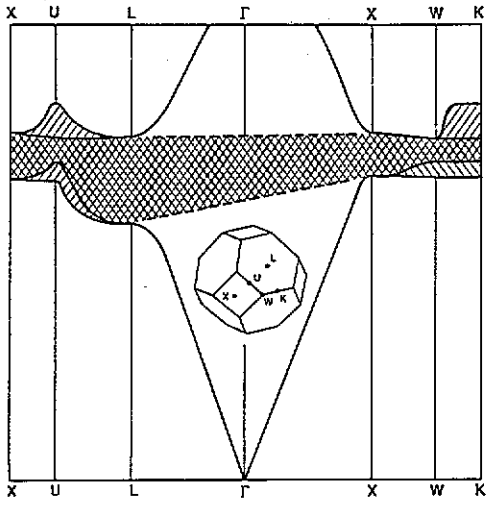

Figure 12. The purported photonic band structure of the spherical void structure shown in figure 8(*a*). The right-sloping lines represent polarization parallel to the X plane, while the left-sloping lines represent the orthogonal polarization, which has a partial component out of the X plane. The cross-hatched region is the reported photonic band gap. The figure fails to show the crossing of the valence and conduction bands at the W point, which was first discovered by theory.

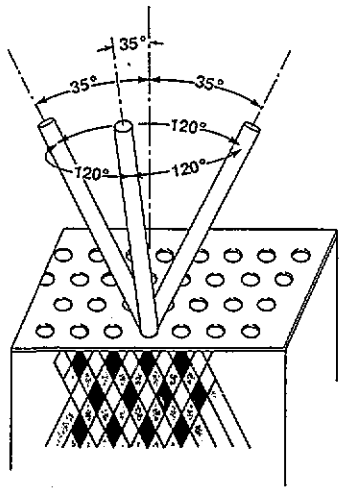

Figure 13. The method of constructing an FCC lattice of the Wigner–Seitz cells as shown in figure 8(*b*). A slab of material is covered by a mask consisting of a triangular array of holes. Each hole is drilled through three times, at an angle 35.26° away from normal, and spread out 120° on the azimuth. The resulting criss-cross of holes below the surface of the slab, suggested by the cross-hatching shown here, produces a fully three-dimensionally periodic FCC structure, with unit cells as given by figure 8(*b*). The drilling can be done by a real drill bit for microwave work, or by reactive ion etching to create an FCC structure at optical wavelengths.

While we were busy with the empirical search, theorists began serious efforts to calculate photonic band structure. The most rapid progress was made not by specialists in electromagnetic theory, but by electronic band-structure theorists who were accustomed to solving Schrödinger's equation in three-dimensionally periodic potentials. The early calculations [12–15] were unsuccessful, however. As a short-cut, they treated the electromagnetic field as a scalar, much as is done for electron waves in Schrödinger's

equation. The scalar wave theory of photonic band structure did not agree well with experiment. For example, it predicted photonic band gaps in the dielectric sphere structure, where none were observed experimentally. The approximation of Maxwell's equations as a scalar wave equation was not working. Finally, incorporating the full vector Maxwell's equations, theory began to agree with experiment. Leung [16] was probably the first to publish a successful vector wave calculation in photonic band structure, followed by others [17, 18], with substantially similar results. The theorists agreed well with one another, and they agreed well with experiment [11], except at the high-degeneracy points U and, particularly, W. What the experiment failed to see was the degenerate crossing of valence and conduction bands at those points.

The unexpected pseudo-gap in the FCC crystal triggered concern and a search for a way to overcome the problem. A worried editorial [19] was published in *Nature*. But even before the editorial appeared, the problem had already been solved by the Iowa State group of Ho, Chan and Soukoulis [18]. The degenerate crossing at the W point was very susceptible to changes in symmetry of the structure. If the symmetry was lowered by filling the WS unit cell, not by a single spherical atom, but by two atoms positioned along the ⟨1 1 1⟩ direction as in diamond structure, then a full photonic band gap opened up. Their discovery of a photonic band gap using a diamond 'form factor' is particularly significant since diamond geometry seems to be favoured by Maxwell's equations. A form of diamond structure [20] gives the widest photonic band gaps requiring the least index contrast $n \sim 1.87$.

More generally, the spherical void symmetry in figure 8(a) can be lowered by distorting the spheres along the ⟨1 1 1⟩ direction, lifting the degeneracy at the W point. The WS unit cell in figure 8(b) has great merit for this purpose. Holes are drilled through the top three facets of the rhombic dodecahedron and exit through the bottom three facets. The beauty of the structure in figure 8(b) is that a stacking of WS unit cells results in straight holes that pass clear through the entire 'crystal'! The 'atoms' are odd-shaped, roughly cylindrical voids centred in the WS unit cell, with a preferred axis pointing to the top vertex, ⟨1 1 1⟩. An operational illustration of the construction that produces an FCC 'crystal' of such WS unit cells is shown in figure 13.

A slab of material is covered by a mask containing a triangular array of holes. Three drilling operations are conducted through each hole, 35.26° off normal incidence and spread out 120° on the azimuth. The resulting criss-cross of holes below the surface of the slab produces a fully three-dimensionally periodic FCC structure, with WS unit cells given by figure 8(b)! The drilling can be done by a real drill bit for microwave work, or by reactive ion etching to create an FCC structure at optical wavelengths.

In spite of non-spherical atoms in figure 8(b), the Brillouin zone (BZ) is identical to the standard FCC BZ shown in textbooks. Nevertheless, we have chosen an unusual perspective from which to view the Brillouin zone in figure 14. Instead of having the FCC BZ resting on one of its diamond-shaped facets as is usually done, we have chosen in figure 14 to present it resting on a hexagonal face. Since there is a preferred axis for the atoms, the distinctive L points centred in the top and bottom hexagons are three fold symmetry axes, and are labelled L_3. The L points centred in the other six hexagons are symmetric only under a 360° rotation, and are labelled L_1. It is helpful to know that the U_3–K_3 points are equivalent since they are a reciprocal lattice vector apart. Likewise the U_1–K_1 points are equivalent.

Figure 15 shows the dispersion relations along different meridians for our primary experimental sample of normalized hole diameter $d/a = 0.469$ and 78% volume fraction removed (where a is the unit cube length). The oval points represent experimental data with s polarization ($\perp$ to the plane of incidence, $\parallel$ to the slab surface) while the triangular

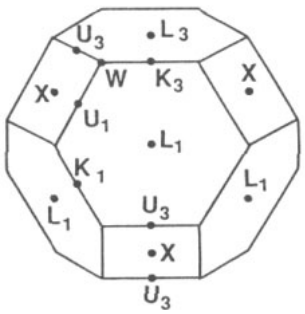

Figure 14. The Brillouin zone of an FCC structure incorporating non-spherical atoms, as in figure 8(*b*). Since the space lattice is not distorted, this is simply the standard FCC Brillouin zone lying on a hexagonal face rather than the usual cubic face. Only the L points on the top and bottom hexagons are three-fold symmetry axes. Therefore, they are labelled L_3. The L points on the other six hexagons are labelled L_1. The U_3–K_3 points are equivalent since they are a reciprocal lattice vector apart. Likewise the U_1–K_1 points are equivalent.

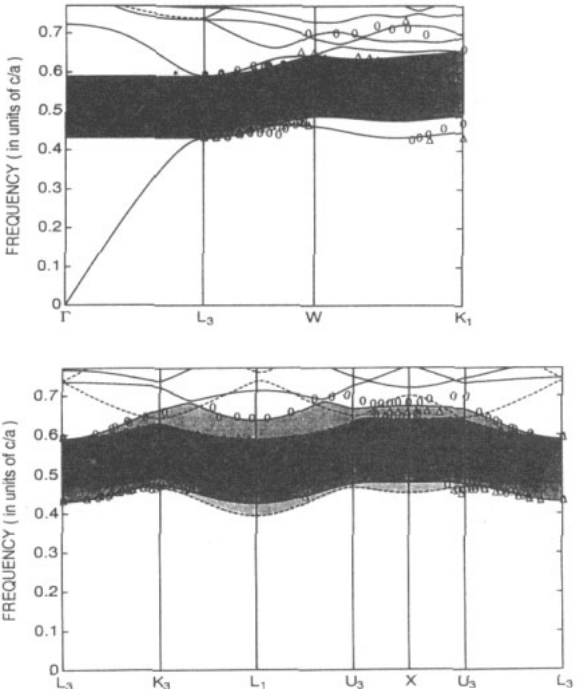

Figure 15. Frequency ω versus wavevector k dispersion along the surface of the Brillouin zone shown in figure 14, where c/a is the speed of light divided by the FCC cube length. The ovals and triangles are the experimental points for s and p polarization respectively. The full and broken curves are the calculations for s and p polarization respectively. The dark shaded band is the totally forbidden band gap. The lighter shaded stripes above and below the dark band are forbidden only for s and p polarization respectively.

points represent p polarization (‖ to the plane of incidence, partially ⊥ to the slab surface). The horizontal abscissa in figure 15(*b*), L_3–K_3–L_1–U_3–X–U_3–L_3, represents a full meridian from the north pole to the south pole of the BZ. Along this meridian the Bloch wavefunctions separate neatly into s and p polarizations. The s and p polarized theory curves are the full and broken curves respectively. The dark shaded band is the totally forbidden photonic band gap. The lighter shaded stripes above and below the dark band are forbidden only for s and p polarization respectively.

At a typical semiconductor refractive index, $n = 3.6$, the 3D forbidden gap width is 19% of its centre frequency. Calculations [21] indicate that the gap remains open for refractive indices as low as $n = 2.1$ using circular holes. We have also measured the imaginary wavevector dispersion within the forbidden gap. At mid-gap we find an attenuation of

10 dB per unit cube length a. Therefore, the photonic crystal need not be very many layers thick to expel effectively the zero-point electromagnetic field. The construction of figure 13 can be implemented by reactive ion etching as shown in figure 16. In reactive ion etching, the projection of circular mask openings at 35° leaves oval holes in the material, which might not perform as well. Fortunately it was found [21], defying 'Murphy's law' that the forbidden gap width for oval holes is actually improved, fully 21.7% of its centre frequency.

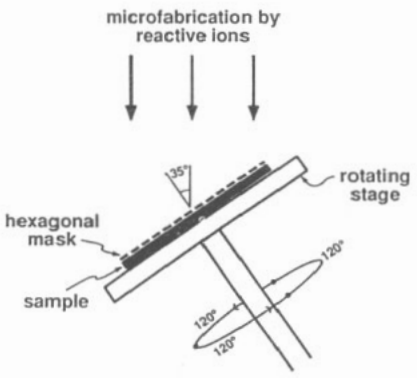

Figure 16. Construction of the non-spherical void photonic crystal of figure 8(*b*) and figures 13–15 by reactive ion etching.

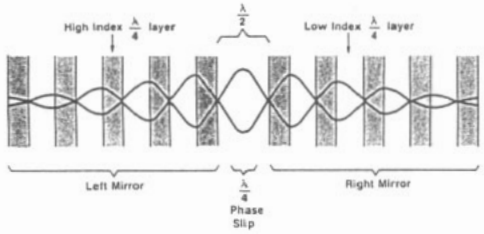

Figure 17. A one-dimensional Fabry–Perot resonator made of multilayer dielectric mirrors with a space of one half-wavelength between the left and right mirrors. The net effect is to introduce a quarter-wavelength phase slip defect into the overall periodic structure. A defect mode is introduced at mid-gap.

4. Doping the photonic crystal

The perfect semiconductor crystal is quite elegant and beautiful, but it becomes ever more useful when it is doped. Likewise, the perfect photonic crystal can become of even greater value when a defect [22] is introduced.

Lasers, for example, require that the perfect 3D translational symmetry should be broken. Even while spontaneous emission into all 4π steradians should be inhibited, a local electromagnetic mode, linked to a defect, is still necessary to accept the stimulated emission. In one-dimensional distributed feedback lasers [23], a quarter-wavelength defect is introduced, forming effectively a Fabry–Perot cavity as shown in figure 17. In three-dimensional photonic band structure, a local defect-induced structure resembles a Fabry–Perot cavity, except that it reflects radiation back upon itself in all 4π spatial directions.

The perfect three-dimensional translational symmetry of a photonic crystal can be lifted in either one of two ways: (i) Extra dielectric material maybe added to one of the unit cells. We find that such a defect behaves very much like a donor atom in a semiconductor. It gives rise to donor modes that have their origin at the bottom of the conduction band. (ii) Conversely translational symmetry can be broken by removing some dielectric material from one of the unit cells. Such defects resemble acceptor atoms in semiconductors. The associated acceptor modes have their origin at the top of the valence band. We will find that acceptor modes are particularly well suited to act as laser micro-resonator cavities. Indeed,

it appears that photonic crystals made of sapphire or other low-loss dielectrics will make the highest-Q single-mode cavities (of modal volume $\sim 1\lambda^3$), covering electromagnetic frequencies above the useful working range of superconducting metallic cavities. The short-wavelength limit in the ultraviolet is set by the availability of optical materials with refractive index $\gtrsim 2$, the threshold index [18, 21] for the existence of a photonic band gap.

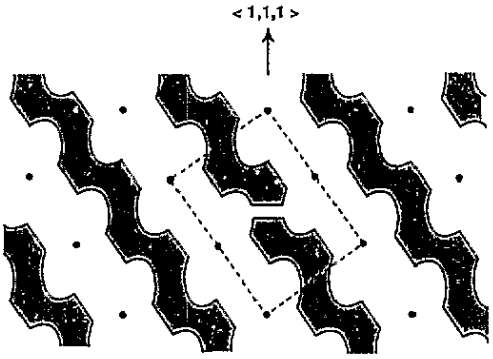

Figure 18. A $\langle 1\,\bar{1}\,0\rangle$ cross-sectional view of our face-centred cubic photonic crystal consisting of non-spherical 'air-atoms' centred on the dots. Dielectric material is represented by the shaded area. The rectangular broken line is a face diagonal cross section of the unit cube. Donor defects consisted of a dielectric sphere centred on an atom. We selected an acceptor defect as shown centred in the unit cube. It consists of a missing horizontal slice in a single vertical rib.

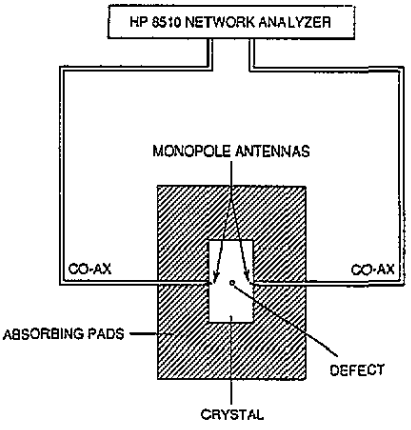

Figure 19. Experimental configuration for the detection of local electromagnetic modes in the vicinity of a lattice defect. Transmission amplitude attenuation from one antenna to the other is measured. At the local mode frequency the signal hops by means of the local mode in the centre of the photonic crystal, producing a local transmission peak. The signal propagates in the $\langle 1\,1\,1\rangle$ direction through 8–10 atomic layers.

Figure 18 is $\langle 1\,\bar{1}\,0\rangle$ cross section of our photonic crystal, (of figure 8(b) and figures 13–15), cutting through the centre of a unit cube. Shading represents dielectric material. The dots are centred on the 'air-atoms' and the rectangular broken line is a face-diagonal cross section of the unit cube. Since we could design the structure at will, donor defects were chosen to consist of a single dielectric sphere centred in an air-atom. Likewise, by breaking one of the interconnecting ribs, it is easy to create acceptor modes. We selected an acceptor defect as shown in figure 18, centred in the unit cube. It comprises a vertical rib that has a missing horizontal slice.

The heart of our experimental apparatus is a photonic crystal embedded in microwave-absorbing pads as shown in figure 19. The photonic crystals were 8–10 crystal layers thick in the $\langle 1\,1\,1\rangle$ direction. Monopole antennae, consisting of 6 mm pins, coupled radiation to the defect mode. The HP 8510 Network Analyzer was set up to measure transmission between the antennae. Figure 20(a) shows the transmission amplitude in the absence of a defect. There is very strong attenuation ($\sim 10^{-5}$) between 13 and 16 GHz marking the valence and conduction band edges of the forbidden gap. This is a tribute to both the dynamic range of the network analyser, and the sizable imaginary wavevector in the forbidden gap.

A transmission spectrum in the presence of an acceptor defect is shown in figure 20(b). Most of the spectrum is unaffected, except at the electromagnetic frequency marked 'Deep acceptor' within the forbidden gap. At that precise frequency, radiation 'hops' from the

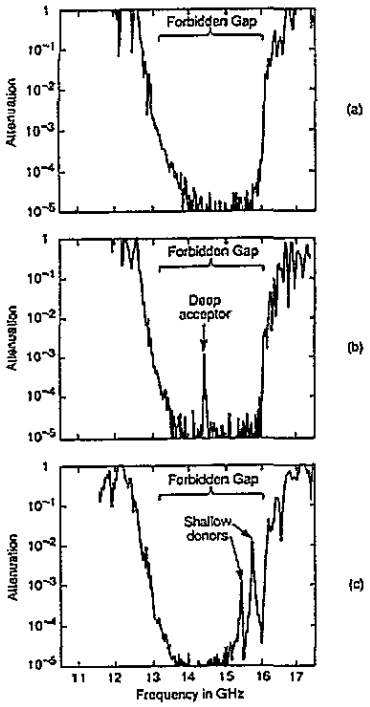

Figure 20. (*a*) Transmission attenuation through a defect-free photonic crystal, as a function of microwave frequency. The forbidden gap falls between 13 and 16 GHz. (*b*) Attenuation through a photonic crystal with a single acceptor in the centre. The large acceptor defect volume shifted its frequency near mid-gap. The electromagnetic resonator Q was $\sim$ 1000, limited only by the loss tangent of the dielectric material. (*c*) Attenuation through a photonic crystal with a single donor defect, an uncentred dielectric sphere, leading to two shallow donor modes.

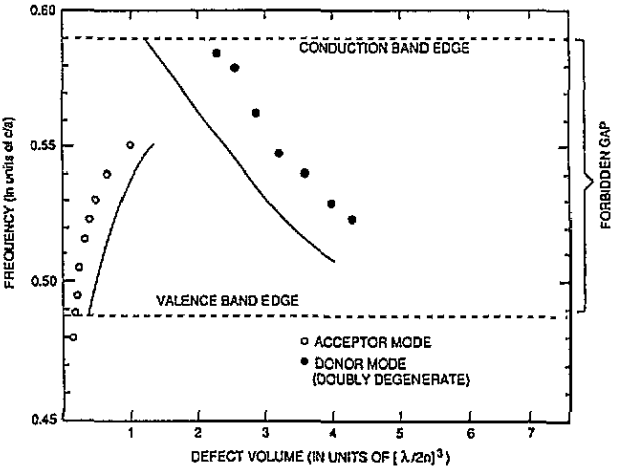

Figure 21. Donor- and acceptor-mode frequencies as a function of normalized donor and acceptor defect volume. The points are experimental and the corresponding curves are calculated. Defect volume is normalized to $(\lambda/2n)^3$, where λ is the mid-gap vacuum wavelength and n is the refractive index. A finite defect volume is required to bind a mode in the forbidden gap.

transmitting antenna to the acceptor mode and then to the receiving antenna. The acceptor-level frequency, within the forbidden gap, is dependent on the volume of material removed. Figure 21 shows the acceptor-level frequency as a function of defect volume removed from one unit cell. When a relatively large volume of material is removed, the acceptor level is deep, as shown in figure 20(*b*). A smaller amount of material removed results in a shallow acceptor level, nearer the valence band. If the removed material volume falls below a threshold volume, the acceptor level falls within the continuum of levels below the top of the valence band, becoming metastable.

On an expanded frequency scale we can measure the resonator Q of the deep acceptor mode, which is $Q \sim 1000$, as limited by the loss tangent of the Emerson & Cumming Stycast material of which the photonic crystal was made.

The behaviour of an off-centre donor defect is shown in figure 20(*c*). In that case the donor volume was only slightly above the required threshold for forming bound donor modes. Already two shallow donor modes can be seen in figure 20(*c*). When the donor is

centred in the Wigner–Seitz unit cell, the two modes merge to form a doubly degenerate donor level as in figure 21. Single donor defects seem to produce multiple donor levels. Figure 21 gives the donor-level frequency as a function of donor volume. As in the case of acceptors, there is a threshold defect volume required for the creation of bound modes below the conduction band edge. However, the threshold volume for donor defects is almost 10 times larger than the acceptor threshold volume. Apparently, this is due to the electric field concentration in the dielectric ribs at the top of the valence band. Bloch wavefunctions at the top of the valence band are rather easily disrupted by the missing rib segment.

We have chosen in figure 21 to normalize the defect volume to a natural volume of the physical system, $(\lambda/2n)^3$, which is basically a cubic half-wavelength in the dielectric medium. More specifically, λ is the vacuum wavelength at the mid-gap frequency, and n is the refractive index of the dielectric medium. Since we are measuring a dielectric volume, it makes sense to normalize to a half-wavelength cube as measured at the dielectric refractive index. Based on the reasonable scaling of figure 21, our choice of volume normalization would seem justified.

The vertical rib with a missing horizontal slice, as in figure 18, can be readily microfabricated. It should be possible to create it in III–V materials by growing an aluminium-rich epitaxial layer and lithographically patterning it down to a single dot the size of one of the vertical ribs. After regrowth of the original III–V composition and reactive ion etching of the photonic crystal, HF acid etching, whose [24] selectivity $\geqslant 10^8$, will be used to remove the Al-rich horizontal slice from the one rib containing such a layer. The resonant frequency of the microcavity can be controlled by the thickness of the Al-rich sacrificial layer.

Therefore, by doping the photonic crystal, it is possible to create high-Q electromagnetic cavities whose modal volume is less than a half-wavelength cubed. These doped photonic crystals would be similar to metallic microwave cavities, except that they would be usable at higher frequencies where metal cavity walls would become lossy. Using sapphire as a dielectric, for example it should be possible to make a millimetre-wave cavity with $Q \gtrsim 10^9$. The idea is not to compete directly with superconducting cavities, but rather to operate at higher frequencies, where the superconductors become lossy. Given the requirement for refractive index > 2, doped photonic crystals should work well up to ultraviolet wavelengths where diamond crystal and TiO_2 are still transparent.

5. Applications

The forthcoming availability of single-mode microcavities at optical frequencies will lead to a new situation in quantum electronics. Of course, microwave cavities containing a single electromagnetic mode have been known for a long time. At microwave frequencies, however, spontaneous emission of electromagnetic radiation is a weak and unimportant process. At optical frequencies, spontaneous emission comes into its own. Now we can combine the physics and technology of spontaneous emission with the capability for single-mode microcavities at optical frequencies where spontaneous emission is important. This combination is fundamentally a new regime in quantum electronics.

The major example of this new type of device is the single-mode light-emitting diode (SM LED), which can have many of the favourable coherence properties of lasers, while being a more reliable and threshold-less device. Progress in electromagnetic microcavities allows all the spontaneous emission of a LED to be funnelled into a single electromagnetic mode.

As the interest in low-threshold semiconductor laser diodes has grown, e.g. for optical interconnects, its spontaneously luminescent half-brother, the light-emitting diode, has begun to re-emerge in a new form. In this new form the LED is surrounded by an optical cavity. The idea is for the optical cavity to make available only a single electromagnetic mode for the output spontaneous emission from the semiconductor diode. In fact the figure-of-merit for such a cavity is β, the fraction of spontaneous emission that is being funnelled into the desired mode. What is new for this application is the prospective ability to make high-β cavities at optical frequencies employing photonic crystals. The three-dimensional character of the cavities ensures that spontaneous emission will not seek out those neglected modes which are found propagating in a direction away from the optical confinement.

With all the spontaneous emission funnelled into a single optical mode, the SM LED can begin to have many of the coherence and statistical properties normally associated with above-threshold lasing. The essential point is that the spontaneous emission factor β should approach unity. (A closely related concept is that of the 'zero-threshold laser', in which the high spontaneous emission factor produces a very soft and indistinct threshold characteristic in the light output versus current input curve of laser diodes.) The idea is to combine the advantages of the LED, which is threshold-less and highly reliable with those of the semiconductor laser, which is coherent and very efficient.

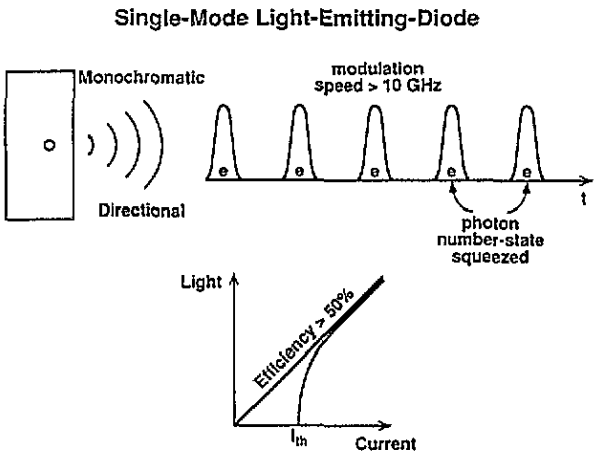

Figure 22. An illustration of the properties of the single-mode light-emitting diode (SM LED), whose cavity is represented by the small circle inside the rectangular photonic crystal, at left. The words 'monochromatic' and 'directional' represent the temporal and spatial coherence of the SM LED output as explained in the text. The modulation speed can be > 10 GHz, and the differential quantum efficiency can be > 50%, competitive with laser diodes. But there is no threshold current for the SM LED as indicated in the L versus I curves at the bottom. The regular stream of photoelectrons, e, is meant to represent photon-number-state squeezing, which can be produced by the SM LED if the spontaneous emission factor β of the cavity is high enough.

The coherence properties of the SM LED are illustrated in figure 22. In a laser, single-mode emission is the result of gain saturation and mode competition. In the SM LED, there is no gain and therefore no gain saturation, but the output is still single-mode, because only one mode is available for emission. Since a single spatial mode can always be mode-converted into a plane wave, the SM LED can be regarded as having spatial coherence.

What about temporal coherence? The spectral linewidth of the SM LED is narrower than the luminescence band of the semiconductor. All the radiation is funnelled into the narrow spectral band determined by the microcavity Q. Thus SM LED have both spatial and temporal coherence as represented by words 'directional' and 'monochromatic' in figure 22.

What about the modulation speed of SM LED in comparison to laser diodes under direct-current modulation? Generally, the modulation speed depends on the carrier lifetime. Since electron–hole pairs in laser diodes experience both spontaneous and simulated

recombination, they have an advantage. However, single-mode cavities concentrate zero-point electric field fluctuations into a smaller volume, creating a stronger matrix element for spontaneous emission. Detailed calculations indicate that spontaneous emission can be speeded up by a factor ~ 10 due to this cavity quantum-electrodynamic (QED) effect. On figure 22 we indicate that a modulation speed > 10 GHz should be possible for SM LED.

The same cavity QED effects can enhance the spontaneous emission efficiency of SM LED since the radiative rate can then compete more successfully with non-radiative rates. External efficiency should exceed 50%, but this can come most easily from intelligent LED design [25] rather than cavity QED effects.

Shown at the bottom of figure 22 is the light output versus current input curve of SM LED and laser diodes. An SM LED can compete with a laser diode in terms of differential external efficiency, but the SM LED can have the advantage by not demanding any threshold current. Lack of threshold behaviour makes the output power and the operating wavelength of an SM LED relatively insensitive to ambient temperature. Combined with the inherent reliability of a LED, this should produce many systems advantages for the SM LED concept.

The final SM LED property illustrated in figure 22 is photon-number-state squeezing, as suggested by the regular sequence of photoelectrons on the horizontal line. Stimulated emission is *not* required for these exotic squeezing effects. The critical variable is absolute quantum efficiency. If the quantum efficiency of the SM LED is high, then these useful correlations will exist in the spontaneous output of the single-mode LED. This requires, most of all, a high spontaneous emission factor β, our overall figure-of-merit for microcavities.

There are many other applications for photonic crystals, particularly in the microwave and millimetre-wave regime. They are very imaginative, and they have gone far beyond our initial goals for using photonic crystals in quantum optics.

6. Conclusion

It is worth while to summarize the similarities and the differences between photonic band structure (PBS) and electronic band structure (EBS). This is best done by reference to table 1.

Table 1. A summary of the differences and similarities between photonic band structure and electronic band structure.

	Electronic band structure	Photonic band structure
Underlying dispersion relation	parabolic	linear
Angular momentum	spin 1/2 scalar wave approximation	spin 1 vector wave character
Accuracy of band theory	approximate due to electron–electron interactions	essentially exact

Electrons are massive, and so the underlying dispersion relation for electrons in crystals is parabolic. Photons have no mass, so the underlying dispersion relation is linear. But as

a result of the periodicity, the photons develop an effective mass in PBS, and this should come as very little surprise.

Electrons have spin 1/2, but frequently this is ignored, and Schrödinger's equation is treated in a scalar wave approximation. In electronic band theory the spin 1/2 is occasionally important, however. In contrast, photons have spin 1, but it is generally never a good approximation to neglect polarization in PBS calculations.

Finally, we come to the accuracy of band theory. It is sometimes believed that band theory is always a good approximation in electronic structure. This is not really true. When there are strong correlations, as in the high-T_c superconductors, band theory is not even a good zeroth-order approximation. Photons are highly non-interacting, so, if anything, band theory makes more sense for photons than for electrons.

The final point to make about photonic crystals is that they are very empty structures, consisting of about 78% empty space. But in a sense they are much emptier than that. They are emptier and quieter than even the vacuum, since they contain not even zero-point fluctuations within the forbidden frequency band.

Acknowledgments

I would like to thank John Gural for drilling all the holes and Tom Gmitter for making the measurements. Thanks are also due to Ming Leung and Bob Meade for their collaborative work. The Iowa State group is thanked for making me aware of their diamond structure results prior to publication.

References

[1] Yablonovitch E 1987 *Phys. Rev. Lett.* **58** 2059
[2] John S 1987 *Phys. Rev. Lett.* **58** 2486
[3] Yamamoto Y, Machida S and Richardson W H 1992 *Science* **255** 1219
[4] Purcell E M 1946 *Phys. Rev.* **69** 681
[5] Drexhage K H 1974 *Progress in Optics* vol 12, ed E Wolf (Amsterdam: North-Holland) see p 165
[6] Bykov V P 1975 *Sov. J. Quantum Electron.* **4** 861
[7] Hulet R G, Hilfer E S and Kleppner D 1985 *Phys. Rev. Lett.* **55** 2137
[8] Van der Ziel A 1954 *Noise* (Engelwood Cliffs, NJ: Prentice-Hall) see pp 208–9
[9] Sozuer H S, Haus J W and Inguva R 1992 *Phys. Rev.* B **45** 13962
[10] Darwin C G 1914 *Phil. Mag.* **27** 675
[11] Yablonovitch E and Gmitter T J 1989 *Phys. Rev. Lett.* **63** 1950
[12] Satpathy S, Zhang Z and Salehpour M R 1990 *Phys. Rev. Lett.* **64** 1239
[13] Leung K M and Liu Y F 1990 *Phys. Rev.* B **41** 10188
[14] John S and Rangarajan R 1988 *Phys. Rev.* B **38** 10101
[15] Economu E N and Zdersis A 1989 *Phys. Rev.* B **40** 1334
[16] Leung K M and Liu Y F 1990 *Phys. Rev. Lett.* **65** 2646
[17] Zhang Z and Satpathy S 1990 *Phys. Rev. Lett.* **65** 2650
[18] Ho K M, Chan C T and Soukoulis C M 1990 *Phys. Rev. Lett.* **65** 3152
[19] Maddox J 1990 *Nature* **348** 481
[20] Chan C T, Ho K M and Soukoulis C M 1991 *Europhys. Lett.* **16** 563
[21] Yablonovitch E, Gmitter T J and Leung K M 1991 *Phys. Rev. Lett.* **67** 2295
[22] Yablonovitch E, Gmitter T J, Meade R D, Rappe A M, Brommer K D and Joannopoulos J D 1991 *Phys. Rev. Lett.* **67** 3380
[23] Haus H A and Shank C V 1976 *IEEE J. Quantum Electron.* **QE-12** 532
McCall S L and Platzman P M 1985 *IEEE J. Quantum Electron.* **QE-21** 1899
[24] Yablonovitch E, Gmitter T, Harbison J P and Bhat R 1987 *Appl. Phys. Lett.* **51** 2222
[25] Schnitzer I, Yablonovitch E, Caneau C and Gmitter T J 1993 *Appl. Phys. Lett.* **62** 131